1

# Modeling the Physical Phenomena Involved by Laser Beam – Substance Interaction

Marian Pearsica, Stefan Nedelcu, Cristian-George Constantinescu,
Constantin Strimbu, Marius Benta and Catalin Mihai
*"Henri Coanda" Air Force Academy*
*Romania*

## 1. Introduction

The mathematical model is based on the heat transfer equation, into a homogeneous material, laser beam heated. Because transient phenomena are discussed, it is necessary to consider simultaneously the three phases in material (solid, liquid and vapor), these implying boundary conditions for unknown boundaries, resulting in this way analytical and numerical approach with high complexity.
Because the technical literature (Belic, 1989; Hacia & Domke, 2007; Riyad & Abdelkader, 2006) does not provide a general applicable mathematical model of material-power laser beam assisted by an active gas interaction, it is considered that elaborating such model, taking into account the significant parameters of laser, assisting gas, processed material, which may be particularized to interest cases, may be an important technical progress in this branch. The mathematical methods used (as well the algorithms developed in this purpose) may be applied to study phenomena in other scientific/technical branches too. The majority of works analyzing the numerical and analytical solutions of heat equation, the limits of applicability and validity of approximations in practical interest cases, is based on results achieved by Carslaw and Jaeger using several particular cases (Draganescu & Velculescu, 1986; Dowden, 2009, 2001; Mazumder, 1991; Mazumder & Steen, 1980).
The main hypothesis basing the mathematical model elaboration, derived from previous research team achievements (Pearsica et al., 2010, 2009; Pearsica & Nedelcu, 2005), are: laser processing is a consequence of photon energy transferred in the material and active gas jet, increasing the metal destruction process by favoring exothermic reactions; the processed material is approximated as a semi-infinite region, which is the space limited by the plane $z = 0$, the irradiated domain being much smaller than substance volume; the power laser beam has a "Gaussian" type radial distribution of beam intensity (valid for $TEM_{00}$ regime); laser beam absorption at z depth respects the Beer law; oxidations occurs only in laser irradiated zone, oxidant energy being "Gaussian" distributed; the attenuation of metal vapors flow respects an exponential law. One of the mathematical hypothesis needing a deeper analysis is the shape of the boundaries between liquid and vaporization, respectively liquid and solid states, supposed as previously known, the parameters characterizing them being computed in the thermic regime prior to the calculus moment.
The laser defocusing effect, while penetrating the processed metal is taken into consideration too, as well as energy losses by electromagnetic radiation and convection. The

proposed method solves simultaneously the heat equation for the three phases (solid, liquid and vapor), computing the temperature distribution in material and the depth of penetration of the material for a given processing time, the vaporization speed of the material being measurable in this way.

## 2. Analytical model equations

The invariant form of the heat equation for an isotropic medium is given by (1).

$$\frac{c_v \cdot \rho}{k} \frac{\partial T}{\partial t} = \Delta T \tag{1}$$

where: $\rho\,[kg/m^3]$ is the mass density; $c_v [J \cdot kg^{-1} \cdot K^{-1}]$ – volumetric specific heat; $T[K]$ – temperature; $k[W \cdot m^{-1} \cdot K^{-1}]$ – heat conductivity of the material; $t[s]$ – time; $\Delta$ – Laplace operator.

Because the print of the laser beam on the material surface is a circular one, thermic phenomena produced within the substantial, have a cylindrical symmetry. Oz is considered as symmetry axis of the laser beam, the object surface equation is $z = 0$ and the positive sense of Oz axis is from the surface to the inside of the object. The heat equation within cylindrical coordinates $(\theta, r, z)$ will be:

$$\frac{1}{K} \frac{\partial T}{\partial t} = \frac{1}{r^2} \frac{\partial^2 T}{\partial \theta^2} + \frac{1}{r} \frac{\partial}{\partial r} \left( r \frac{\partial T}{\partial r} \right) + \frac{\partial^2 T}{\partial z^2} \tag{2}$$

where: $K[m^2/s]$ is the diffusivity of the material.

Limit and initial conditions are attached to heat equation according to the particularly cases which are the discussed subject. These conditions are time and space dependent. In time, the medium submitted to the actions of the laser presents the solid, liquid and vapor state separated by previously unknown boundaries. A simplifying model taking into consideration these boundaries, by considering them as having a cylindrical symmetry, was proposed. By specifying the pattern D, the temperature initial conditions and the conditions on D pattern boundaries, one can have the solution of heat equation, T(x,y,z,t) for a certain substantial.

### 2.1 Temperature source modeling

The destruction of the crystalline network of the material and its vaporization, along the pre-established curve, is completed by the energy of photons created inside the material, and by the jet of the assisting gas ($O_2$). This gas intensifies the material destroying action due to the exothermic reactions provided. Dealing with a semi-infinite solid heated by a laser beam uniform absorbed in its volume, it is assumed that Beer law governs its absorption at z depth. It is considered a radial "Gaussian" distribution of the laser beam intensity, which corresponds to the central part of the laser beam. It is assumed that photons energy is totally transformed in heat. So, the heat increasing rate, owing the photons energy, at z depth (under surface) is given by:

$$\frac{dQ}{dt \cdot dV} = h\nu \cdot \sigma \cdot \rho \cdot I(r,z) \quad = \frac{P_L}{\pi d^2 \cdot l} e^{-\left[\left(\frac{r}{d}\right)^2 + \frac{z}{l}\right]} \tag{3}$$

where: $dV[m^3]$ and $dt[s]$ are the infinitesimal volume and time respectively, $\sigma[m^2/kg]$ – the absorption cross section, $\sigma = 1/\rho \cdot l$, $I(rt)[W/m^2]$ – photons distribution in material volume, $l[m]$ – the attenuation length of laser radiation, $P_L[W]$ – the laser power; $\pi d^2[m^2]$ – irradiated surface, $r[m]$ – radial coordinate, and $h\nu[J]$ – the energy of one photon.
The vaporized material diffuses in oxygen atmosphere and oxidizes exothermic, resulting in this way an oxidizing energy, which appears as an additional kinetic energy of the surface gas constituents, leading to an additional heating of the laser processed zone. It is assumed an exponential attenuation of the metal vapors flow and oxidizing is only inner laser irradiated zone, the oxidizing energy being "Gaussian" distributed. The rate of oxidizing energy release on the material is given by (4):

$$\frac{dQ_{ox}}{dt \cdot dV} = \eta_o \cdot \sigma_{ox} \cdot \rho \cdot n_{o_2} \cdot v_s \cdot \frac{\varepsilon}{M} e^{\left[\frac{z}{l_{ox}} - \left(\frac{r}{d}\right)^2\right]} \tag{4}$$

where: $\eta_o$ is the oxidizing efficiency, $\varepsilon[J]$ – oxidizing energy on completely oxidized metal atom, $\sigma_{ox}[m^2/kg]$ – effective oxidizing section, $n_{o_2}[m^{-3}]$ – oxygen atomic concentration, $v_s[m/s]$ – vaporization boundary speed, $M[kg]$ – atomic mass of metal, and $l_{ox}[m]$ – oxidizing length, $l_{ox} = 1/(n_{o_2} \cdot \sigma_{ox})$. In (4), z is negative outside the material, so the attenuation is obvious. The full temperature source results as a sum of (3) and (4), and assuming a constant vaporization boundary speed, the instantaneous expression of temperature source is given by (Pearsica et al., 2010):

$$S(r,z) = e^{-\left(\frac{r}{d}\right)^2} \cdot \left[\frac{P_L}{\pi d^2 \cdot l} e^{-\frac{z - v_s \cdot t}{l}} \cdot h(z - v_s \cdot t) + \eta_o \frac{\varepsilon \cdot \rho \cdot v_s}{M \cdot l_{ox}} e^{-\frac{v_s \cdot t - z}{l_{ox}}} \cdot h(v_s \cdot t - z)\right] \tag{5}$$

where h(x) is Heaviside function. In temperature source expression, z origin is the same with the vaporization boundary, which advance in profoundness as the material is drawn. The spatial and temporal temperature distribution in material is governed by the full temperature source and results by solving the heat equation.

### 2.2 Boundary and initial conditions for heat equation

a. Dirichlet conditions

Let $S_1 \subset S$. For $S_1$ surface points it is assumes that the temperature T is known as a function f(M,t), and the remaining surface, S, the temperature is constant, $T_a$:

$$T(M,t) = \begin{cases} f(M,t), & M \in S_1 \\ T_a, & M \in S \setminus S_1 \end{cases} \tag{6}$$

b. Neumann conditions

Let $S_2 \subset S$. It is known the derivate in the perpendicular n direction to the surface $S_2$:

$$\frac{\partial T(M,t)}{\partial n} = g(M,t), \quad M \in S_2 \tag{7}$$

c. Initial conditions

It is assumed that at $t = t_o$ time is known the thermic state of the material in D pattern:

$$T(M,t_o)=T_o(M),\quad M\in D \tag{8}$$

In time, successions the phases the object suffers while irradiate by the power laser beam are the following:

- phase 1, for $0\le t<t_{top}$;
- phase 2, for $t_{top}\le t<t_{vap}$;
- phase 3, for $t\ge t_{vap}$, where $t_{top}$ and $t_{vap}$ are the starting time moments of the melting, respectively vaporization of the material.

The surfaces separating solid, liquid and vapor state are previously unknown and will be determined using the conditions of continuity of thermic flow on separation surfaces of two different substantial, knowing the temperature and the speed of separation surface (Mazumder & Steen, 1980; Shuja et al., 2008; Steen & Mazumder, 2010).

The isotropic domain D is assumed to be the semi-space $z\ge 0$, so its border, S, is characterized by the equation $z=0$. The laser beam acts on the normal direction, developing thermic effects described by (1). In the initial moment, $t=0$, the domain temperature is the ambient one, $T_a$. If the laser beam radius is d and axis origin is chosen on its symmetry axis, then the condition of type (7) (thermic flow imposed on the surface of the processed material) yields:

$$\left.\frac{\partial T}{\partial x}\right|_{z=0}=\begin{cases}-\dfrac{1}{k}\varphi_S(M,t), & x^2+y^2\le d^2,\ z=0\\ 0, & x^2+y^2>d^2,\ z=0\end{cases} \tag{9}$$

where $\varphi_S(M,t)[W/m^2]$ is the power flow on the processed surface, corresponding to the solid state:

$$\varphi_S(M,t)=\frac{A_S\cdot P_L}{\pi d^2}e^{-\left(\frac{r}{d}\right)^2},\quad r^2=x^2+y^2,\ z=0 \tag{10}$$

where: $A_S$ is the absorbability of solid surface, and $P_L[W]$ – the power of laser beam.

Regarding the working regime, two kinds of lasers were taken into consideration: continuous regime lasers ($P_L$ = constant) and pulsated regime lasers ($P_L$ has periodical time dependence, governed by a "Gaussian" type law). If the laser pulse period is $t_p=t_{on}+t_{off}$, then the expression used for the laser power is the following:

$$P_L=\begin{cases}C\left[e^{-\frac{1}{4}}-e^{-\left(\frac{t-\frac{t_{on}}{2}-k\,t_p}{t_{on}}\right)^2}\right], & t\in\left[k\,t_p,\ k\,t_p+t_{on}\right];\ k\in N\\ 0, & t\in\left((k+1)t_p-t_{off},\ (k+1)t_p\right)\end{cases} \tag{11}$$

where: $C=P_{L\max}\cdot e^{1/4}$. Due to the cylindrical symmetry, $\frac{\partial^2 T}{\partial\theta^2}=0$, so (2) changes to:

$$\frac{1}{K}\frac{\partial T}{\partial t}=\frac{1}{r}\frac{\partial T}{\partial r}+\frac{\partial^2 T}{\partial r^2}+\frac{\partial^2 T}{\partial z^2} \tag{12}$$

Equations (6) and (7) will be:

$$T(r,z,0)=T_a,\quad (r,z)\in[0,\ r_\infty]\times[0,\ r_\infty] \tag{13}$$

$$\frac{\partial T(r,0,t)}{\partial z}=\begin{cases}-\frac{1}{k}\varphi(r,0,t), & r\le d\\ 0, & r>d\end{cases} \tag{14}$$

Because it was assumed that the area of thermic influence neighboring the processing is comparable to the processing width it may consider that $r_\infty \approx 6d$, and is valid the relation (Dirichlet condition):

$$T(r_\infty,z,t)=T_a,\quad z>0 \tag{15}$$

In order to avoid the singularity in $r=0$ it is considered that:

$$\frac{\partial T(0,z,t)}{\partial r}=0 \tag{16}$$

The power flow on the processed surface corresponding to the solid state is given by the relation (10).

As a result of laser beam action, the processed material surface heats, the temperature reaching the melting value, $T_{top}$ at a certain moment of time. The heating goes on, so in another moment of time, the melted material temperature reaches the vaporization value, $T_{vap}$. That moment onward the vapor state appears in material. The equations (12), (13), (14), and (15) still govern the heating process in all of three states (solid, liquid and vapor), changing the material constants k and K, which will be denoted according to the state of the point M(r,z), as it follows: $k_1$, $K_1$ – for the solid state, $k_2$, $K_2$ – for the liquid state, respectively $k_3$, $K_3$ – for the vapor state.

The three states are separated by time varying boundaries. To know these boundaries is essential to determine the thermic regime at a certain time moment. If the temperature is known, then the following relations describe the boundaries separating the processed material states:

- solid and liquid states boundary:

$$T(r,z,t)=T_{top},\quad (r,z)\in C_l(t) \tag{17}$$

- liquid and vapor states boundary:

$$T(r,z,t)=T_{vap},\quad (r,z)\in C_v(t) \tag{18}$$

The material temperature rises from $T_{top}$ to $T_{vap}$ between the boundaries $C_l(t)$ and $C_v(t)$. The power flow on the processed surface corresponding to the liquid state is given by:

$$\varphi_L(M,t)=\frac{A_L\cdot P_L}{\pi d^2}e^{-\left(\frac{r}{d}\right)^2},\quad r^2=x^2+y^2,\ z=0 \tag{19}$$

where $A_L$ is the absorbability on liquid surface.
The power flow on the processed surface corresponding to vapor state is given by:

$$\varphi_V(M,t)=C_G\cdot e^{-\left(\frac{r}{d_V}\right)^2},\quad r^2=x^2+y^2,\ z=z_f \tag{20}$$

where: $C_G=C_{G_1}+C_{G_2}=\frac{P_L}{\pi d_V^2}+\frac{\eta_o\cdot\varepsilon\cdot\rho_v\cdot v_S}{M}$ ($d_V[m]$ – radius of the laser beam on the separation boundary between vapor state and liquid state and it is calculated with the relation (21), $z_f$ – z coordinate corresponding to the boundary between vapor state and liquid state; $C_{G_2}$ is considered only in the vapor state, because the vaporized metal diffusing in atmosphere suffers an exothermic air oxidation, thus resulting an oxidizing energy which provides supplemental heating of the laser beam processed zone).

$$d_V=d+\frac{D-d}{f}\cdot z_f \tag{21}$$

where: $D[m]$ is the diameter of the generated laser beam and $f[m]$ is the focusing distance of the focusing system.
In (14), the power losses through electromagnetic radiation, $\varphi_r[W/m^2]$ and convection, $\varphi_c[W/m^2]$ were taken into account (Pearsica et al., 2008a, 2008b):

$$\varphi_r=\sigma_b\left(T_{vap}^4-T_a^4\right),\ \varphi_c=H\left(T_{vap}-T_a\right) \tag{22}$$

where: $\sigma_b$ is Stefan-Boltzmann constant, H – substantial heat transfer constant. The emittance of irradiated area was considered as equal to 1.

### 2.3 Separating boundaries equations

To solve analytical the presented problem is a difficult task. The method described bellow is a numerical one. An iterative process will be used to find the surfaces $C_l(t)$ and $C_v(t)$. An inverse method was applied, choosing the boundaries as surfaces with rotational symmetry, ellipsoid type (Pearsica et al., 2008a, 2008b). Because the rotational ellipsoid is characterized by a double parametrical equation:

$$\frac{r^2}{\alpha^2}+\frac{z^2}{\beta^2}=1 \tag{23}$$

it's enough to know the points $(r_1,z_1)$ and $(r_2,z_2)$ on the considered surface in order to determine the parameters $\alpha$ and $\beta$. The points $(r(t),0)$ and $(0,z(t))$, with $r(t_{top})=r^*$ and $z(t_{top})=z^*$ were chosen, where $t_{top}$ is the time moment when the temperature is $T_{top}$.
On the surface $C_l(t)$ is known the equation relating temperature gradient and the surface movement speed in this (normal) direction:

$$\frac{\partial T}{\partial n} = -\frac{\rho_2 L_2}{k_2} v_n \tag{24}$$

where: $k_2[W \cdot m^{-1} \cdot K^{-1}]$ is the heat conductivity that belongs to liquid state, $L_2[J/kg]$ – the latent melting heat, $\rho_2[kg/m^3]$ – the mass density that belongs to liquid state, and $v_n[m/s]$ is the movement speed of the boundary surface, $C_1(t)$, in the direction of its external normal vector $\bar{n}$.

The boundary at the t moment is supposed as known, respectively the points $(r(t), 0)$ and $(0, z(t))$ on it. It is enough to determine the points $(r(t+\Delta t), 0)$ and $(0, z(t+\Delta t))$ in order to find $C_1(t+\Delta t)$. In the point $(r(t), 0)$, (24) yields:

$$\frac{\partial T}{\partial r} = -\frac{\rho_2 L_2}{k_2} v_r \;\Rightarrow\; v_r = -\frac{k_2}{\rho_2 L_2}\frac{\partial T}{\partial r} \tag{25}$$

where: $\frac{\partial T}{\partial r} = \frac{T(r+\Delta r) - T_{top}}{\Delta r}$

It obtains:

$$r(t+\Delta t) = r(t) + v_r \cdot \Delta t \tag{26}$$

In $(0, z(t))$ point, (24) yields:

$$\frac{\partial T}{\partial z} = -\frac{\rho_2 L_2}{k_2} v_z \;\Rightarrow\; v_z = -\frac{k_2}{\rho_2 L_2}\frac{\partial T}{\partial z} \tag{27}$$

where: $\frac{\partial T}{\partial z} = \frac{T(z+\Delta z) - T_{top}}{\Delta z}$. It results:

$$z(t+\Delta t) = z(t) + v_z \cdot \Delta t \tag{28}$$

The new boundary parameters, $\alpha(t+\Delta t)$ and $\beta(t+\Delta t)$, are returned by (26) and (28):

$$\alpha(t+\Delta t) = r(t+\Delta t),\;\; \beta(t+\Delta t) = z(t+\Delta t) \tag{29}$$

The moment $t_{top}$ is the first time when the above procedure is applied. $z(t_{top}) = 0$ and $r(t_{top}) = 0$ at this moment of time. Because the temperature gradient (having the z direction,) is known in $z = 0$ and $r = 0$:

$$\left.\frac{\partial T}{\partial z}\right|_{z=0} = -\frac{1}{k_1}\varphi_L(0,0,t) \tag{30}$$

in (28) results:

$$z(t_{top} + \Delta t) = \frac{\varphi_L(0,0,t)}{\rho_2 L_2}\Delta t \tag{31}$$

where $\varphi_L$ is the power flow on the processed surface corresponding to the liquid state. In these conditions, (26) becomes:

$$r\left(t_{top}+\Delta t\right)=\frac{T_{top}-T\left(\Delta r\right)}{\Delta r\cdot\rho_2\cdot L_2}k_2\cdot\Delta t \tag{32}$$

The same procedure is applied to find the $C_v(t)$ boundary, taking into account the latent heat of vaporization $L_3[J/kg]$, the mass density corresponding to vapor state $\rho_3[kg/m^3]$ and respectively the heat conductivity corresponding to vapor state $k_3[W\cdot m^{-1}\cdot K^{-1}]$.

### 2.4 Digitization of heat equation, boundary and initial conditions

The first step of the mathematical approach is to make the equations dimensionless (Mazumder, 1991; Pearsica et al., 2008a, 2008c). In heat equation case it will be achieved by considering the following ($r_\infty$ and $z_\infty$ are the studied domain boundaries, where the material temperature is always equal to the ambient one):

$$r=x r_\infty,\quad z=y r_\infty,\quad T=T_a u,\quad t=\frac{r_\infty^2}{K_1}\tau \tag{33}$$

The heat equation (12) in the new variables $x$, $y$, $\tau$, and u yields:

$$\frac{1}{x}\frac{\partial u}{\partial x}+\frac{\partial^2 u}{\partial x^2}+\frac{\partial^2 u}{\partial y^2}=\frac{K_1}{K_i}\frac{\partial u}{\partial\tau},\quad (x,y)\in[0,1]\times[0,1],\quad \tau\geq 0,\text{ and } i=1,2,3 \tag{34}$$

The initial and limit conditions for the unknown function, u yield:

- phase 1, for $0\leq t<t_{top}$

$$u(x,y,0)=1,\quad (x,y)\in[0,1]\times[0,1] \tag{35}$$

$$u(1,y,\tau)=1,\quad y\in[0,1],\quad \tau\in[0,\tau_{top}],\quad \tau_{top}=\frac{K_1}{r_\infty^2}t_{top} \tag{36}$$

$$u(x,1,\tau)=1,\quad x\in[0,1],\quad \tau\in[0,\tau_{top}] \tag{37}$$

- phase 2, for $t_{top}\leq t<t_{vap}$

$$u(0,0,\tau_{top})=u_{top} \tag{38}$$

$$u(x,y,\tau_{top})=u_1(x,y,\tau_{top}),\quad (x,y)\in(0,1]\times(0,1] \tag{39}$$

where: $\tau_{top}$ is the $\tau$ value when $u=u_{top}$, $u_{top}=T_{top}/T_a$, and $u_1(x,y,\tau_{top})$ is the heat equation solution in according to phase 1.

If $\tau\in[\tau_{top},\tau_{vap})$ both solid and liquid phases coexist in material, occupying $D_s(\tau)$ and $D_l(\tau)$ domains respectively, which are separated by a time varying boundary, $C_l(\tau)$, so $u(x,y,\tau)=u_{top}$ on it. The projection of the domain $D_l(\tau)$ on $y=0$ plane is the set $\{x/x\leq x_1\}$. For $x=1$ and $y=1$ respectively, the conditions are:

$$u(1,y,\tau)=u(x,1,\tau)=1 \tag{40}$$

Phase 2 is going on while $\tau\in[\tau_{top},\tau_{vap})$, where: $\tau_{vap}=\frac{t_{vap}\cdot K_1}{r_\infty^2}$.

- phase 3, for $t\geq t_{vap}$

$$u(0,0,\tau_{vap})=u_{vap} \tag{41}$$

$$u(x,y,\tau_{vap})=u_2(x,y,\tau_{vap}),\ \ (x,y)\in D_l(\tau_{vap})\setminus(0,0) \tag{42}$$

$$u(x,y,\tau_{vap})=u_1(x,y,\tau_{vap}),\ \ (x,y)\in D_s(\tau_{vap}) \tag{43}$$

where $u_2(x,y,\tau_{vap})$ is the heating equation solution from phase 2. In this temporal phase all the three (solid, liquid and vapor) states coexist in material, occupying the domains: $D_s(\tau)$, $D_l(\tau)$ and $D_v(\tau)$, separated by mobile boundaries $C_l(\tau)$ and $C_v(\tau)$, on which $u(x,y,\tau)=u_{vap}$. The projection of the domains $D_l(\tau)$ and $D_v(\tau)$ on plane $y=0$ are the sets: $\{x/x\in[x_2,x_1]\}$ and $\{x/x\in[0,x_2]\}$. According to phase 3, the conditions on $y=0$ surface (Neumann type conditions) are:

a. $x_2\leq x_1\leq\frac{d}{r_\infty}$:

$$\frac{\partial u}{\partial y}=\begin{cases}-\frac{r_\infty}{T_a\cdot k_3}\left[\varphi_V(x,y_f,\tau)-\varphi_r-\varphi_c\right], & x\in[0,x_2]\\ -\frac{r_\infty}{T_a\cdot k_2}\varphi_L(x,0,\tau), & x\in(x_2,x_1]\\ -\frac{r_\infty}{T_a\cdot k_1}\varphi_S(x,0,\tau), & x\in\left(x_1,\frac{d}{r_\infty}\right]\\ 0, & x\in\left(\frac{d}{r_\infty},1\right]\end{cases} \tag{44}$$

b. $x_2\leq\frac{d}{r_\infty}\leq x_1$:

$$\frac{\partial u}{\partial y}=\begin{cases}-\frac{r_\infty}{T_a\cdot k_3}\left[\varphi_V(x,y_f,\tau)-\varphi_r-\varphi_c\right], & x\in[0,x_2]\\ -\frac{r_\infty}{T_a\cdot k_2}\varphi_L(x,0,\tau), & x\in\left(x_2,\frac{d}{r_\infty}\right]\\ 0, & x\in\left(\frac{d}{r_\infty},1\right]\end{cases} \tag{45}$$

c. $x_2 > \frac{d}{r_\infty}$:

$$\frac{\partial u}{\partial y} = \begin{cases} -\frac{r_\infty}{T_a \cdot k_3}\left[\varphi_V(x, y_f, \tau) - \varphi_r - \varphi_c\right], & x \in \left[0, \frac{d}{r_\infty}\right] \\ 0, & x \in \left(\frac{d}{r_\infty}, 1\right] \end{cases} \tag{46}$$

Similar Neumann type conditions are settled for temporal phases 1 and 2, accordingly to their specific parameters.
For $x = 1$, and $y = 1$ respectively, the conditions are given by (40).

### 2.5 Digitization of equations on separation boundaries

The speed of time variation of separation boundaries, $v_n$, is given by (47), where n is the external normal vector of the boundary.

$$v_n = -\frac{k_e}{\rho_e \cdot L_e}\frac{\partial T}{\partial n}, \quad e = 2,3 \tag{47}$$

For $y = 0$ and $x = x_f$, it results:

$$v_r(x_f, 0) = -\frac{k_e}{\rho_e \cdot L_e}\frac{\partial T}{\partial r} = -\frac{k_e \cdot T_a}{\rho_e \cdot L_e \cdot r_\infty}\frac{\partial u}{\partial x}, \quad e = 2,3 \tag{48}$$

respectively,

$$v_r(x_f, 0) = \frac{dr}{dt} = \frac{K_1}{r_\infty}\frac{dx}{d\tau} \tag{49}$$

It results:

$$\frac{dx}{d\tau} = -\frac{k_e \cdot T_a}{\rho_e \cdot L_e \cdot K_1}\frac{\partial u}{\partial x}, \quad e = 2,3 \tag{50}$$

The $\alpha$ parameter of separation boundary at $\tau + \Delta\tau$ moment is:

$$\alpha = x_f(\tau + \Delta\tau) = x_f(\tau) + \frac{dx}{d\tau}\Delta\tau = x_f(\tau) - \frac{k_e \cdot T_a}{\rho_e \cdot L_e \cdot K_1}\frac{\partial u}{\partial x}\Delta\tau, \quad e = 2,3 \tag{51}$$

where:

$$\frac{\partial u}{\partial x} \approx \frac{u(x_k, 0) - u(x_f, 0)}{x_k - x_f} \tag{52}$$

where $x_k \in$ digitization network. For $\tau = \tau_{top}$ and $\tau = \tau_{vap}$ respectively, (52) yields:

$$\frac{\partial u}{\partial x} = \frac{u_1(x_1, 0) - u_{top}}{x_1}, \quad x_f(\tau_{top}) = 0 \tag{53}$$

$$\frac{\partial u}{\partial x}=\frac{u_2(x_1,0)-u_{vap}}{x_1},\quad x_f(\tau_{vap})=0 \tag{54}$$

For $x=0$ and $y=y_f$, it results:

$$v_z(0,y_f)=-\frac{k_e}{\rho_e\cdot L_e}\frac{\partial T}{\partial z}=-\frac{k_e\cdot T_a}{\rho_e\cdot L_e\cdot r_\infty}\frac{\partial u}{\partial y},\quad e=2,3 \tag{55}$$

respectively,

$$v_z(0,y_f)=\frac{dz}{dt}=\frac{K_1}{r_\infty}\frac{dy}{d\tau} \tag{56}$$

It results:

$$\frac{dy}{d\tau}=-\frac{k_e\cdot T_a}{\rho_e\cdot L_e\cdot K_1}\frac{\partial u}{\partial y},\quad e=2,3 \tag{57}$$

The $\beta$ parameter of separation boundary at $\tau+\Delta\tau$ moment is:

$$\beta=y_f(\tau+\Delta\tau)=y_f(\tau)+\frac{dy}{d\tau}\Delta\tau=y_f(\tau)-\frac{k_e\cdot T_a}{\rho_e\cdot L_e\cdot K_1}\frac{\partial u}{\partial y}\Delta\tau,\quad e=2,3 \tag{58}$$

where:

$$\frac{\partial u}{\partial y}\approx\frac{u(0,y_k)-u(0,y_f)}{y_k-y_f} \tag{59}$$

For $\tau=\tau_{top}$ it results:

$$\frac{\partial u}{\partial y}=-\frac{r_\infty}{T_a\cdot k_2}\varphi_L(0,0,\tau_{top}),\quad y_f(\tau_{top})=0 \tag{60}$$

For $\tau=\tau_{vap}$ it results:

$$\frac{\partial u}{\partial y}=-\frac{r_\infty}{T_a\cdot k_3}\left[\varphi_V(0,0,\tau_{top})-\varphi_r-\varphi_c\right],\quad y_f(\tau_{vap})=0 \tag{61}$$

## 3. Determination of temperature distribution in material

Using the finite differences method, the domain $[0,1]\times[0,1]$ is digitized by sets of equidistant points on Ox and Oy directions (Pearsica et al., 2008a, 2008b).

### 3.1 Digitization of mathematical model equations

In the network points, the partial derivatives will be approximated by:

$$\left.\frac{\partial u}{\partial x}\right|_{(i,j)}\approx\frac{u_{i+1,j}-u_{i-1,j}}{2\Delta x},\quad \left.\frac{\partial^2 u}{\partial x^2}\right|_{(i,j)}\approx\frac{u_{i+1,j}-2u_{i,j}+u_{i-1,j}}{(\Delta x)^2} \tag{62}$$

$$\left.\frac{\partial u}{\partial y}\right|_{(i,j)} \approx \frac{u_{i,j+1}-u_{i,j-1}}{2\Delta y},\quad \left.\frac{\partial^2 u}{\partial y^2}\right|_{(i,j)} \approx \frac{u_{i,j+1}-2u_{i,j}+u_{i,j-1}}{(\Delta y)^2} \tag{63}$$

$$\left.\frac{\partial u}{\partial \tau}\right|_{(i,j)} \approx \frac{u_{i,j}(\tau+\Delta\tau)-u_{i,j}(\tau)}{\Delta\tau} \tag{64}$$

With these approximations, in each inner point of the network the partial derivatives equations become an algebraic system such:

$$a^j_{i,i-1}u_{i-1,j}+a^j_{i,i}u_{i,j}+a^j_{i,i+1}u_{i+1,j}+b^j_{i,i}u_{i,j-1}+c^j_{i,i}u_{i,j+1}=f_{i,j} \tag{65}$$

The system coefficients are linear expressions of the partial derivatives equation, computed in the network points. If there are M and N points on Ox and Oy axis respectively, the system will include $M\times N$ equations with $(M+1)\times(N+1)$ unknowns. Adding the conditions for the domain boundaries, the system is determinate.

The implicit method, involving evaluations of the equation terms containing spatial derivatives at $\tau+\Delta\tau$ moment, is used to obtain the unknown function $u(x,y,\tau)$ distribution in network points. The option is on this method because there are no restrictions on choosing the time and spatial steps $(\Delta\tau,\Delta x,\Delta y)$. According to this method, an additional index is introduced, representing the time moment. With these explanations, the heat equation with finite differences yields:

$$\left[\frac{1}{x}\frac{\partial u}{\partial x}+\frac{\partial^2 u}{\partial x^2}+\frac{\partial^2 u}{\partial y^2}\right]_{i,j,n+1}=\frac{K_1}{K_e}\left(\frac{\partial u}{\partial \tau}\right)_{i,j,n+1},\quad e=1,2,3 \tag{66}$$

Finally, the algebraic system yields:

$$\lambda_1\left(1-\frac{\Delta x}{2x_i}\right)u_{i-1,j,n+1}-\left[\frac{K_1}{K_e}+2\lambda_1(1+\lambda_2)\right]u_{i,j,n+1}+\lambda_1\left(1+\frac{\Delta x}{2x_i}\right)u_{i+1,j,n+1}+$$
$$+\lambda_1\lambda_2 u_{i,j-1,n+1}+\lambda_1\lambda_2 u_{i,j+1,n+1}=-u_{i,j,n}\cdot\frac{K_1}{K_e},\quad e=1,2,3 \tag{67}$$

where: $\lambda_1=\frac{\partial\tau}{(\Delta x)^2}$, $\lambda_2=\left(\frac{\Delta x}{\Delta y}\right)^2$, and $x_i=x_o+(i-1)\cdot\Delta x$. The value $x_o$ is very close to zero and it was chosen to avoid the singularity appearing in heating equation at $x=0$. Formally, this singularity appears because if $x=0$, then $\frac{\partial u}{\partial x}=0$ too. If $\Delta x=1/M$ and $\Delta y=1/N$ will result $i=\overline{1,M+1}$ and $j=\overline{1,N+1}$.

Equation (67) will be written for $i=\overline{2,M}$ and $j=\overline{2,N}$. In case $j=N+1$ and $i=M+1$, the constraints imposed to u are:

$$u_{i,N+1,n+1}=1,\quad u_{M+1,j,n+1}=1 \tag{68}$$

The initial condition is for $n=0$:

$$u_{i,j,1}=1,\ \ \forall(i,j) \tag{69}$$

For $i=1$, $j\neq 1$, (67) is still valid, observing that $u_{0,j,n+1}=u_{2,j,n+1}$, because the solution is symmetrical related to $x=0$. In this case, (67) yields:

$$-\left[\frac{K_1}{K_e}+2\lambda_1(1+\lambda_2)\right]u_{1,j,n+1}+2\lambda_1 u_{2,j,n+1}+\lambda_1\lambda_2 u_{1,j-1,n+1}+\lambda_1\lambda_2 u_{1,j+1,n+1}=$$

$$=-u_{1,j,n}\cdot\frac{K_1}{K_e},\ \ e=1,2,3 \tag{70}$$

For $j=1$, when writing the initial conditions for the boundary $y=0$, the temporal phase of the material must be taken into account. Only the equations corresponding to the third phase ($t\geq t_{vap}$) will be presented, because it is the most complex one, all the three states (solid, liquid and vapor) being taken into account. Similar results were obtained for the other two phases, in a similar way, accordingly to their influencing parameters. The initial conditions are:

$$u_{1,1,n_0}=u_{vap},\quad \tau_{vap}=\Delta\tau\cdot n_0 \tag{71}$$

$$u_{i,j,n_0}=u^{(2)}_{i,j,n_0},\quad (x_i,y_j)\in D_1\setminus(0,0) \tag{72}$$

$$u_{i,j,n_0}=u^{(1)}_{i,j,n_0},\quad (x_i,y_j)\in D_s \tag{73}$$

where $u^{(2)}$ is the solution of the problem corresponding to the second temporal phase ($t_{top}\leq t<t_{vap}$).
The boundary corresponding to the $n_0+1$ time moment will be determined hereinafter. The parameters of the boundary separating the vapor and liquid will be:

$$\alpha_{n_0+1}=\frac{T_a\cdot k_3\cdot\Delta\tau}{K_1\cdot\rho_v\cdot L_3\cdot\Delta x}\left(u_{1,1,n_0}-u_{2,1,n_0}\right),\ \ \beta_{n_0+1}=\frac{r_\infty\cdot\Delta\tau}{\rho_v\cdot L_3\cdot K_1}\varphi_V(0,0,\tau) \tag{74}$$

The boundary equation will be:

$$x=\frac{\alpha_{n_0+1}}{\beta_{n_0+1}}\sqrt{\beta^2_{n_0+1}-y^2} \tag{75}$$

The boundary separating liquid and solid phases exists at the moment $n_0$, as well at a certain moment n, its parameters being given by (51) and (58). The situation corresponding to the third phase is illustrated in figure 1.
In the marked points, the heating equation must be changed, because its related partial derivatives approximation by using finite differences is not possible anymore (the associated Taylor series in A and B will be used, where $AC=a\Delta x$ and $BC=b\Delta y$). In order

to know if a point is nearby the boundary previously determined, the points $(x_i^{'}, y_i^{'})$ and $(x_j^{''}, y_j^{''})$ respectively will be obtain by intersecting the network lines $(x_i = x_o + (i-1)\Delta x,$ $y_j = (j-1)\Delta y)$ and the boundary $x = \frac{\alpha}{\beta}\sqrt{\beta^2 - y^2}$. It results $h = \left[\frac{y_i^{'}}{\Delta y}\right] + 1$ (floor() + 1) as solution of the equation $(h-1)\Delta y = y_i^{'}$, and:

$$b_p(i,h) = \frac{y_i^{'}}{\Delta y} - \left[\frac{y_i^{'}}{\Delta y}\right], \quad b_m(i,h) = 1, \quad b_m(i,h+1) = 1 - b_p(i,h), \quad b_p(i,h+1) = 1 \tag{76}$$

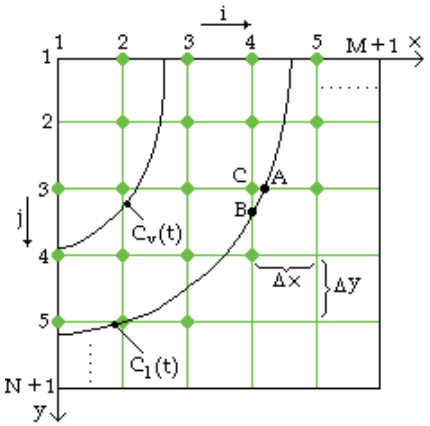


Fig. 1. The boundaries separating the phases

It results (similar) $k = \left[\frac{x_j^{''}}{\Delta x}\right] + 1$ as solution of the equation $(k-1)\Delta x = x_j^{''}$, and:

$$a_p(k,j) = \frac{x_j^{''}}{\Delta x} - \left[\frac{x_j^{''}}{\Delta x}\right], \quad a_m(k,j) = 1, \quad a_m(k+1,j) = 1 - a_p(k,j), \quad a_p(k+1,j) = 1 \tag{77}$$

For the regular points (the ones which are not nearby the boundary), the above mentioned parameters will be:

$$b_p(i,j) = b_m(i,j) = a_p(i,j) = a_m(i,j) = 1 \tag{78}$$

The unified heating equation in a network point (i, j) will be:

$$\frac{2\lambda_1}{a_m(a_m+a_p)}\left(\frac{a_p\Delta x}{2x_i} - 1\right)u_{i-1,j,n+1} + \left(\frac{K_1}{K_3} + \frac{a_m - a_p}{a_m a_p}\frac{\lambda_1\Delta x}{x_i} + \frac{2\lambda_1}{a_m a_p} + \frac{2\lambda_1\lambda_2}{b_m b_p}\right)u_{i,j,n+1} -$$
$$-\frac{\lambda_1(2x_i + a_m\Delta x)}{a_p(a_m+a_p)x_i}u_{fx,n+1} - \frac{2\lambda_1\lambda_2}{b_m(b_p+b_m)}u_{i,j-1} - \frac{2\lambda_1\lambda_2}{b_p(b_m+b_p)}u_{fy,n+1} = u_{i,j,n}\cdot\frac{K_1}{K_3} \tag{79}$$

where the coefficients $a_m$, $a_p$, $b_m$, and $b_p$ depends on point (i, j), and $u_{fx} = u_{i+1,j}$ and $u_{fy} = u_{i,j+1}$, if the point where derivatives are approximated is not nearby the boundary. For $i = 1$, (79) becomes:

$$\left(\frac{K_1}{K_e}+\frac{2\lambda_1}{a_p a_m}+\frac{2\lambda_1\lambda_2}{b_p b_m}-\frac{a_p-a_m}{a_p a_m}\frac{\lambda_1\cdot\Delta x}{x_i}\right)u_{1,j,n+1}+\frac{2\lambda_1}{a_p+a_m}\left(\frac{a_p\Delta x}{2a_m x_i}-\frac{1}{a_m}-\frac{a_m\Delta x}{2a_p x_i}-\right.$$
$$\left.-\frac{1}{a_p}\right)u_{2,j,n+1}-\frac{2\lambda_1\lambda_2}{b_m(b_m+b_p)}u_{1,j-1,n+1}-\frac{2\lambda_1\lambda_2}{b_p(b_m+b_p)}u_{1,j+1,n+1}=u_{1,j,n}\cdot\frac{K_1}{K_e} \tag{80}$$

There are as well vapor, liquid and solid zones on the boundary $y = 0$. Depending on the position of the intersecting points between boundary and $y = 0$, the following situations may occur:

a. $x_1 \le \frac{d}{r_\infty}$:

$$u_{i,1,n+1}-u_{fr}=\frac{\Delta y\cdot a_m\cdot r_\infty}{T_a\cdot k_3}\varphi_V(x_i,y_f,\tau),\quad x_i\in[0,x_2] \tag{81}$$

$$u_{i,1,n+1}-u_{i,2,n+1}=\frac{\Delta y\cdot r_\infty}{T_a\cdot k_2}\varphi_L(x_i,0,\tau),\quad x_i\in(x_2,x_1] \tag{82}$$

$$u_{i,1,n+1}-u_{i,2,n+1}=\frac{\Delta y\cdot r_\infty}{T_a\cdot k_1}\varphi_S(x_i,0,\tau),\quad x_i\in\left(x_1,\frac{d}{r_\infty}\right] \tag{83}$$

b. $x_2 \le \frac{d}{r_\infty} < x_1$:

$$u_{i,1,n+1}-u_{fr}=\frac{\Delta y\cdot a_m\cdot r_\infty}{T_a\cdot k_3}\varphi_V(x_i,y_f,\tau),\quad x_i\in[0,x_2] \tag{84}$$

$$u_{i,1,n+1}-u_{i,2,n+1}=\frac{\Delta y\cdot r_\infty}{T_a\cdot k_2}\varphi_L(x_i,0,\tau),\quad x_i\in\left(x_2,\frac{d}{r_\infty}\right] \tag{85}$$

c. $x_2 > \frac{d}{r_\infty}$:

$$u_{i,1,n+1}-u_{fr}=\frac{\Delta y\cdot a_m\cdot r_\infty}{T_a\cdot k_3}\varphi_V(x_i,y_f,\tau),\quad x_i\in\left[0,\frac{d}{r_\infty}\right] \tag{86}$$

If $x_i > \frac{d}{r_\infty}$, in all of the three mentioned cases:

$$u_{i,1,n+1}=u_{i,2,n+1} \tag{87}$$

Because the discrete network parameters do not influence the initial moment of laser interaction with the material, the temperature gradient on z direction was replaced by the temporal temperature gradient in the initial condition on $z=0$ boundary (Draganescu & Velculescu, 1986). So, the digitized initial condition on $z=0$ boundary yields:

$$u_{i,1,n+1} = u_{i,1,n} + \frac{r_\infty}{k}\sqrt{\frac{K\cdot d\tau}{K_1\cdot n}}\cdot\varphi(x_i,0,\tau) \tag{88}$$

The equations system obtained after digitization and boundary determination will be solved by using an optimized method regarding the solving run time, namely the column wise method. It is an exact type method, preferable to the direct matrix inversing method.

### 3.2 The column wise solving method

From the algebraic system of $(M+1)\times(N+1)$ equations, the minimum dimension will be chosen as unknowns' column dimension. It is assumed to be $M+1$. It is to notice that writing the system in the point $(i,j)$ involves as well the points $(i-1,j),(i+1,j),(i,j-1)$, and $(i,j+1)$ (Pearsica et al., 2008a, 2008b). The system and transformed conditions may be organized, writing in sequence all the equations for each fixed j and variable i, as a vector system. So, by keeping j constant, it results a relationship between columns j, $j-1$, and $j+1$. By denoting $[A_j]$, $[B_j]$, and $[C_j]$ the unknowns coefficients matrixes of the columns j, $j-1$, and $j+1$ respectively, the system for j constant will be:

$$[A_j]\cdot\{U_j\} + [B_j]\cdot\{U_{j-1}\} + [C_j]\cdot\{U_{j+1}\} = \{F_j\} \tag{89}$$

where: [X] is a quadratic matrix, {X} is a column vector, $\{F_j\}$ is the free terms vector, $[A_j]$ is a tri-diagonal matrix whose non-null components are $a_{i,i-1}$, $a_{i,i}$ and $a_{i,i+1}$, and $[B_j]$ and $[C_j]$ are diagonal matrixes. The components of matrixes $[A_j]$, $[B_j]$ and $[C_j]$, are the coefficients of the unified caloric equation written in a point (i,j) of the network, equation (79). The components of $\{F_j\}$ are:

$$f_{i,j} = u_{i,j,n}\cdot\frac{K_1}{K_e},\quad j\neq 1,\quad e=1,2,3 \tag{90}$$

For $j=1$, (90) yields ($[A_1]=[I]$ - unity matrix, and $[B_1]=[C_1]=[0]$):

$$[A_1]\cdot\{U_1\} = \{F_1\} \tag{91}$$

The components of $\{F_1\}$ are computed using the relation:

$$f_{i,1} = \begin{cases} u_{i,1,n} + \dfrac{r_\infty}{k}\sqrt{\dfrac{K\cdot d\tau}{K_1\cdot n}}\cdot\varphi(x_i,0,\tau), & i\le i_d \\ u_{i,1,n}, & i>i_d \end{cases} \tag{92}$$

where $i_d$ is the laser beam limit. Taking into account the relation linking two successive columns, $U_{j-1}$ and $U_j$:

$$\{U_{j-1}\} = [E_j] \cdot \{U_j\} + \{R_j\} \tag{93}$$

and by denoting:

$$[T_j] = ([A_j] + [B_j] \cdot [E_j])^{-1} \tag{94}$$

The following relation results:

$$\{U_j\} = -[T_j] \cdot [C_j] \cdot \{U_{j+1}\} + [T_j](\{F_j\} - [B_j] \cdot \{R_j\}) \tag{95}$$

By comparing (93) and (95) the recurrence relations to find matrixes $[E_j]$ and $\{R_j\}$ yield:

$$[E_{j+1}] = -[T_j] \cdot [C_j], \quad \{R_{j+1}\} = [T_j](\{F_j\} - [B_j] \cdot \{R_j\}) \tag{96}$$

The initial matrixes $[E_1]$ and $\{R_1\}$ are chosen so that (92) is respected:

$$[E_1] = [0], \quad \{R_j\} = \{0\} \tag{97}$$

A sequence determination of the matrixes $[E_j]$ and $\{R_j\}$ till $j = N + 1$ and then, using (93) of $\{U_N\}$, $\{U_{N-1}\}$,…,$\{U_2\}$, bases the computing process. The simplified logical diagram of the function computing the temperature distribution in material is shown in figure 2.

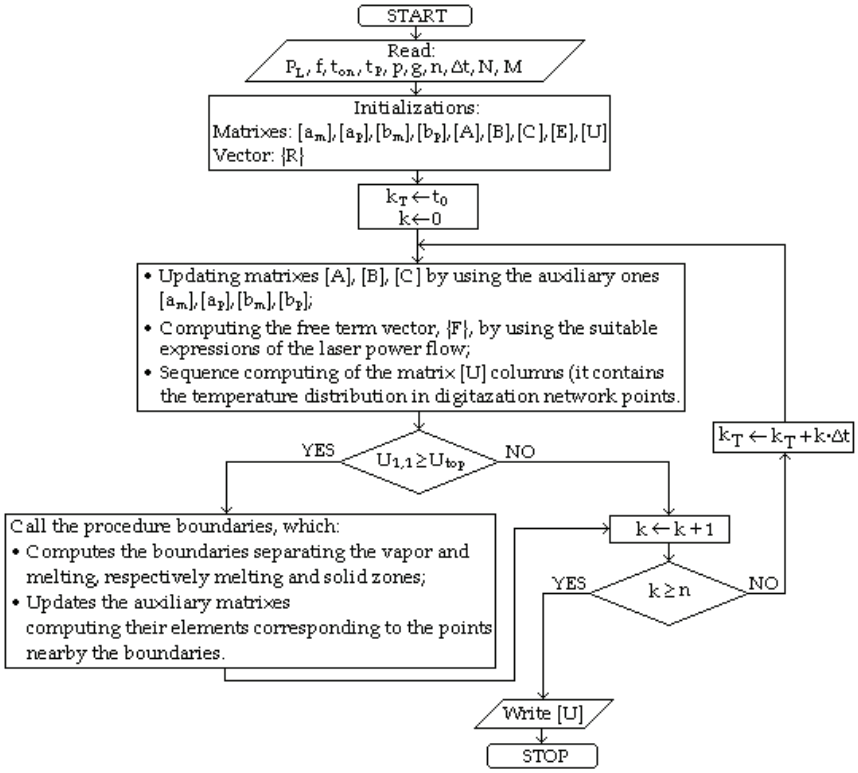


Fig. 2. Logical diagram of the function computing the temperature distribution in material

Input data: $P_L$ - laser power, f - focal distance of the focusing system, $t_{on}$ - laser pulse duration, $t_p$ - laser pulse period, p - additional gas pressure, g - material thickness, n - number of time steps that program are running for, $\Delta t$ - time step, M, N - number of digitization network in Ox and Oy directions, respectivelly.
Both procedures (the main function and the procedure computing the boundaries) were implemented as MathCAD functions.

## 4. Numeric results

The model equations were solved for a cutting process of metals with a high concentration of iron (steel case). In table 1 is presented the temperature distribution in material, computed in continuous regime lasers, with the following input data: $P_L = 1\text{kW}$ (laser power), $\eta_o = 0.74$ (oxidizing efficiency), $p = 0.8\text{bar}$ (additional gas pressure), $d = 0.16\text{mm}$ (focalized laser beam radius), $D = 10\text{mm}$ (diameter of the generated laser beam), $f = 145\text{mm}$ (focal distance of the focusing system), $g = 6\text{mm}$ (material thickness) $A_S = 0.49$ (absorbability on solid surface), $A_L = 0.68$ (absorbability on liquid surface), $\Delta t = 10^{-5}\text{s}$ (time step), $t = 10\text{ms}$ (operation time), $M = 8$ (number of intervals on x direction), $N = 32$ (number of intervals on y direction), $k_T = 1000$ (number of iterations). The iron material constants were taken into consideration, accordingly to the present (solid, liquid or vapor) state.
The real temperatures in material are the below ones multiplied by 25.
Temperature distribution was represented in two situations: at the material surface and at the material evaporating depth $(z = 4.192\text{mm})$ (figure 3).

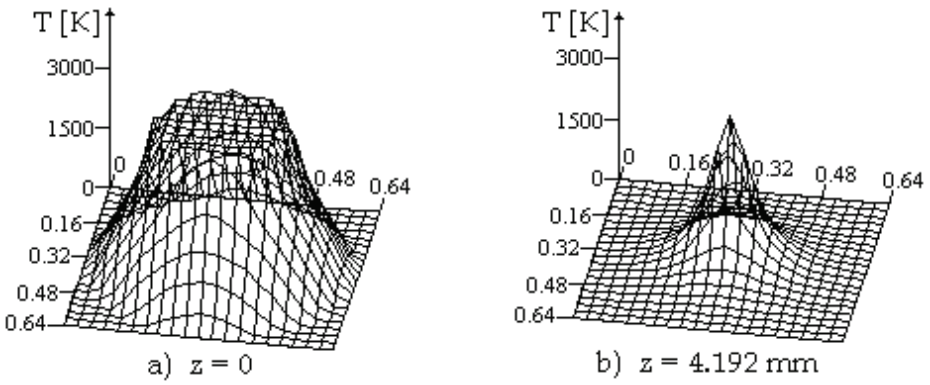


Fig. 3. Temperature distribution, $P_L = 1\text{kW}$, $t = 10\text{ms}$

The depths corresponding to the melting and vaporization temperatures are: $z_{top} = 4.288\text{mm}$, respectively $z_{vap} = 4.192\text{mm}$. The moments when material surface reaches the vaporization and melting temperatures are: $t_{vap} = 0.181 \cdot 10^{-5}\text{s}$, respectively $t_{top} = 0.132 \cdot 10^{-5}\text{s}$. The temperature distributions at different depths within the material, for laser power $P_L = 400\text{W}$, and processing time $t = 1\text{ms}$, are presented in figure 4.

| M<br>N | 1 | 2 | 3 | 4 | 5 | 6 | 7 | 8 | 9 |
|---|---|---|---|---|---|---|---|---|---|
| 1 | 120.3 | 120.3 | 120.3 | 120.3 | 120.3 | 71.6 | 45.0 | 21.4 | 1.0 |
| 2 | 120.3 | 120.3 | 120.3 | 120.3 | 71.6 | 71.6 | 45.0 | 21.4 | 1.0 |
| 3 | 120.3 | 120.3 | 120.3 | 120.3 | 71.6 | 71.7 | 44.8 | 21.3 | 1.0 |
| 4 | 120.3 | 120.3 | 120.3 | 120.3 | 71.6 | 71.6 | 44.7 | 21.3 | 1.0 |
| 5 | 120.3 | 120.3 | 120.3 | 120.3 | 71.6 | 71.6 | 44.3 | 21.1 | 1.0 |
| 6 | 120.3 | 120.3 | 120.3 | 120.3 | 71.6 | 68.4 | 42.1 | 20.1 | 1.0 |
| 7 | 120.3 | 120.3 | 120.3 | 120.3 | 71.6 | 64.9 | 40.0 | 19.1 | 1.0 |
| 8 | 120.3 | 120.3 | 120.3 | 120.3 | 71.6 | 61.7 | 38.0 | 18.2 | 1.0 |
| 9 | 120.3 | 120.3 | 120.3 | 120.3 | 71.6 | 59.0 | 35.4 | 17.4 | 1.0 |
| 10 | 120.3 | 120.3 | 120.3 | 120.3 | 71.6 | 56.8 | 35.0 | 16.8 | 1.0 |
| 11 | 120.3 | 120.3 | 120.3 | 120.3 | 71.6 | 54.9 | 33.9 | 16.3 | 1.0 |
| 12 | 120.3 | 120.3 | 120.3 | 120.3 | 71.6 | 53.4 | 33.0 | 15.8 | 1.0 |
| 13 | 120.3 | 120.3 | 120.3 | 120.3 | 71.6 | 52.2 | 32.3 | 15.5 | 1.0 |
| 14 | 120.3 | 120.3 | 120.3 | 120.3 | 71.6 | 51.3 | 31.7 | 15.2 | 1.0 |
| 15 | 120.3 | 120.3 | 120.3 | 120.3 | 71.6 | 50.3 | 31.0 | 14.9 | 1.0 |
| 16 | 120.3 | 120.3 | 120.3 | 94.9 | 64.4 | 47.2 | 29.5 | 14.2 | 1.0 |
| 17 | 120.3 | 120.3 | 120.3 | 71.6 | 64.0 | 42.5 | 26.0 | 12.5 | 1.0 |
| 18 | 120.3 | 120.3 | 120.3 | 71.6 | 57.3 | 38.3 | 23.5 | 11.4 | 1.0 |
| 19 | 120.3 | 120.3 | 120.3 | 71.6 | 53.1 | 35.2 | 21.4 | 10.3 | 1.0 |
| 20 | 120.3 | 120.3 | 120.3 | 71.6 | 47.4 | 29.6 | 17.4 | 8.4 | 1.0 |
| 21 | 120.3 | 120.3 | 71.6 | 61.2 | 37.5 | 23.2 | 13.5 | 6.5 | 1.0 |
| 22 | 120.3 | 120.3 | 71.6 | 45.0 | 25.8 | 14.7 | 8.0 | 3.9 | 1.0 |
| 23 | 120.3 | 86.0 | 39.3 | 18.7 | 9.2 | 5.0 | 2.9 | 1.7 | 1.0 |
| 24 | 25.6 | 7.6 | 4.2 | 2.7 | 1.9 | 1.5 | 1.2 | 1.1 | 1.0 |
| 25 | 1.5 | 1.3 | 1.2 | 1.1 | 1.1 | 1.0 | 1.0 | 1.0 | 1.0 |
| 26 | 1.0 | 1.0 | 1.0 | 1.0 | 1.0 | 1.0 | 1.0 | 1.0 | 1.0 |
| ... | ... | ... | ... | ... | ... | ... | ... | ... | ... |
| 33 | 1.0 | 1.0 | 1.0 | 1.0 | 1.0 | 1.0 | 1.0 | 1.0 | 1.0 |

Table 1. Temperature distribution in material

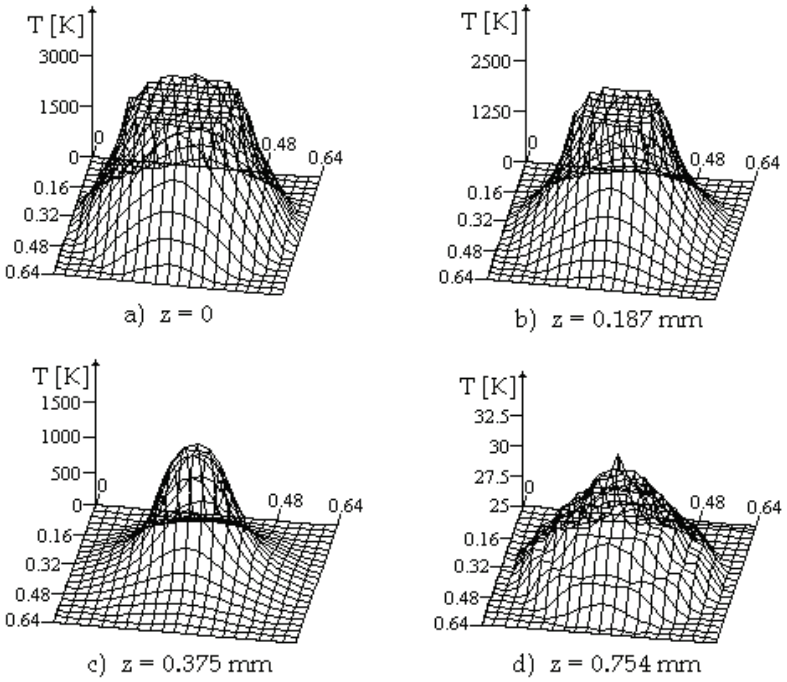


Fig. 4. Temperature distribution, $P_L = 400W$, $t = 1ms$

The temperature distributions on the material surface $(z = 0)$ are quite identical in both mentioned cases (figures 3 and 4). The material vaporization depth is depending on the processing time, and the considered input parameters as well. So, for a 10 times greater processing time and a 2.5 times greater laser power, one may observe a 10.94 times greater vaporization depth, compared with the previous case $(z = 0.383\,mm)$. If comparing the obtained results, it results a quite small dimension of the liquid phase (difference between $z_{top}$ and $z_{vap}$), within $0.006 \div 0.085$ mm.

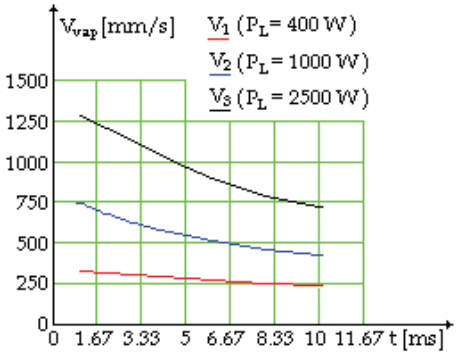


Fig. 5. The vaporization speed variation vs. processing time

Knowing the vaporization depth at a certain processing time allows evaluating the vaporization speed and limited processing speed. The vaporization speed variation as a function of processing time is presented in figure 5. It may be observed that vaporization speed is decreasing function (it decreases as the laser beam advances in material).
The decreasing of the vaporization speed as the vaporization depth increases is owed to the laser beam defocusing effect, which augments once the laser beam advances in material.
The processing speed is computed for a certain material thickness, as a function of vaporization speed corresponding to processing moment when vaporization depth is equal to material thickness. So, for a certain processing time, results the thickness of the material that may be processed, which is equal to vaporization depth.
As a consequence of the mass-flow conserving law, in order to cut a material with a certain thickness, the time requested by moving the irradiated zone must be equal to the time requested by material breakdown. The following relation derives in this way, allowing evaluating the processing speed as a function of vaporization speed:

$$v_T = v_{vap} \cdot \frac{2d}{g} \tag{98}$$

In figure 6 are compared the processing speeds: analytically determined, experimentally determined and returned by the above presented method (Pearsica et al., 2010, 2008c).

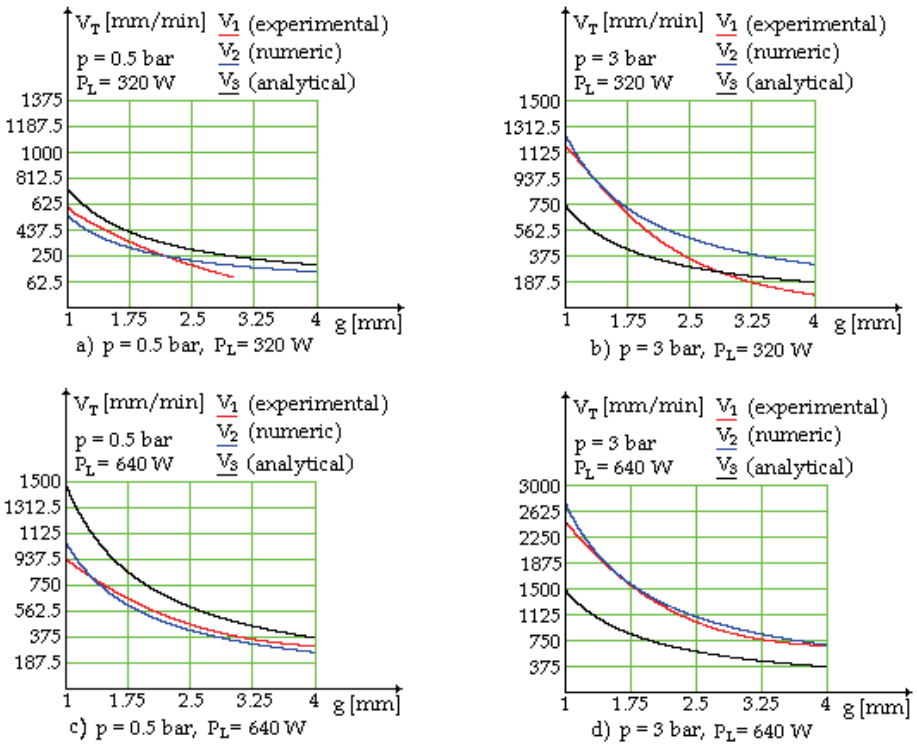


Fig. 6. Processing speed variation

The experimental processing speeds were determined for a general use steel (OL 37), and iron material parameters were considered for the theoretical speeds. It may be observed in the presented figures that processing speed numerical results are a quite good approximation for the experimental ones, for the laser power $P_L = 640\ W$, the maximum error being 11.3% for $p = 3\ bar$ and, 17.28%, for $p = 0.5\ bar$. In case of $P_L = 320\ W$, the numerical determined processing speed matches better the experimental one for small thickness of processed material (for $g = 1\ mm$, the error is 10.2%, for $p = 0.5\ bar$, and 6.89%, for $p = 3\ bar$), the error being greater at bigger thickness (for $g = 3\ mm$ and $p = 0.5\ bar$ the error is 89.4%, and for $g = 4\ mm$ and $p = 3\ bar$ the error is 230.52%).
According to the presented situation, it may be considered that, in comparison with the analytical processing speed, the numerical determined one match better the experiments.

## 5. Conclusion

The computing function allowed determination of: temperature distribution in material, melting depth, vaporization depth, vaporization speed, working speed, returned data allowing evaluation of working and thermic affected zones widths too.
The equations of the mathematical proposed model to describe the way the material submitted to laser action reacts were solved numerically by finite differences method. The algebraic system returned by digitization was solved by using an exact type method, known in literature as column solving method.
The variables and the unknown functions were non-dimensional and it was chosen a net of equidistant points in the pattern presented by the substantial. Because the points neighboring the boundary have distances up to boundary different from the net parameters, some digitization formulas with variable steps have been used for them.
An algebraic system of equation solved at each time-step by column method was obtained after digitization and application of the limit conditions. The procedure is specific to implicit method of solving numerically the heat equation and it was chosen because there were no restrictions on the steps in time and space of the net.
Among the hypothesis on which the mathematics model is based on and hypothesis that need a more thorough analysis is the hypothesis on boundaries formation between solid state and liquid state, respectively, the liquid state and vapor state, supposed to be known previously, parameters that characterize the boundaries being determined from the thermic regime prior to the calculus moment.
The analytical model obtained is experiment dependent, because there are certain difficulties in oxidizing efficiency $\eta_o$ determination, which implies to model the gas-metal thermic transfer mechanism. As well, some material parameters $(c, k, \rho, A_S, ...)$ (which were assumed as constants) are temperature dependent. Their average values in interest domains were considered.
The indirect results obtained as such (the thickness of penetrating the substantial, the vaporization speed) certify the correctness of the hypothesis made with boundary formula. The results thus obtained are placed within the limits of normal physics, which constitutes a verifying of the mathematics model equation.

## 6. Acknowledgment

This work was supported by The National Authority for Scientific Research, Romania – CNCSIS-UEFISCDI: Grant CNCSIS, PN-II-ID-PCE-2008, no. 703/15.01.2009, code 2291:

"Laser Radiation-Substance Interaction: Physical Phenomena Modeling and Techniques of Electromagnetic Pollution Rejection".

## 7. References


Belic, I. (1989). A Method to Determine the Parameters of Laser Cutting. *Optics and Laser Technology*, Vol.21, No.4, (August 1989), pp. 277-278, ISSN 0030-3992

Draganescu, V. & Velculescu, V.G. (1986). *Thermal Processing by Lasers*, Academy Publishing House, Bucharest, Romania

Dowden, J.M. (2009). *The Theory of Laser Materials Processing: Heat and Mass Transfer in Modern Technology*, Springer, ISBN 140209339X, New York, USA

Dowden, J.M. (2001). *The Mathematics of Thermal Modeling*, Chapman & Hall, ISBN 1-58488-230-1, Boca Raton, Florida, SUA

Hacia, L. & Domke, K. (2007). Integral Modeling and Simulating in Some Thermal Problems, *Proceedings of 5th IASME/WSEAS International Conference on Heat and Mass Transfer (THE'07)*, pp. 42-47, ISBN 978-960-6766-00-8, Athens, Greece, August 25-27, 2007

Mazumder, J. (1991). Overview of Melt Dynamics in Laser Processing. *Optical Engineering*, Vol.30, No.8, (August 1991), pp. 1208-1219, ISSN 0091-3286

Mazumder, J. & Steen, W.M. (1980). Heat Transfer Model for C.W. Laser Materials Processing. *Journal of Applied Physics*, Vol.51, No.2, (February 1980), pp. 941-947, ISSN 0021-8979

Pearsica, M.; Baluta, S.; Constantinescu, C.; Nedelcu, S.; Strimbu, C. & Bentea, M. (2010). A Mathematical Model to Compute the Thermic Affected Zone at Laser Beam Processing. *Optoelectronics and Advanced Materials*, Vol.4, No.1, (January 2010), pp. 4-10, ISSN 1842-6573

Pearsica, M.; Constantinescu, C.; Strimbu, C. & Mihai, C. (2009). Experimental Researches to Determine the Thermic Affected Zone at Laser Beam Processing of Metals. *Metalurgia International*, Vol.14, Special issue no.12, (August 2009), pp. 224-228, ISSN 1582-2214

Pearsica, M.; Ratiu, G.; Carstea, C.G.; Constantinescu, C.; Strimbu, C. & Gherman, L. (2008). Heat Transfer Modeling and Simulating for Laser Beam Irradiation with Phase Transformations. *WSEAS Transactions on Mathematics*, Vol.7, No.11, (November 2008), pp. 2174-2180, ISSN 676-685

Pearsica, M.; Ratiu, I.G.; Carstea, C.G.; Constantinescu, C. & Strimbu, C. (2008). Electromagnetic Processes at Laser Beam Processing Assisted by an Active Gas Jet, *Proceedings of 10th WSEAS International Conference on Mathematical Methods, Computational Technique and Intelligent Systems*, pp. 187-193, ISBN 978-960-474-012-3, Corfu, Greece, October 26-28, 2008

Pearsica, M.; Baluta, S.; Constantinescu, C. & Strimbu, C. (2008), A Numerical Method to Analyse the Thermal Phenomena Involved in Phase Transformations at Laser Beam Irradiation, *Journal of Optoelectronics and Advanced Materials*, Vol.10, No.5, (August 2008), pp. 2174-2181, ISSN 1454-4164

Pearsica, M. & Nedelcu, S. (2005). A Simulation Method of Thermal Phenomena at Laser Beam Irradiation, *Proceedings of 10th International Conference „Applied Electronics"*, pp. 269-272, ISBN 80-7043-369-8, Pilsen, Czech Republic, September 7-8, 2005

Riyad, M. & Abdelkader, H. (2006). Investigation of Numerical Techniques with Comparison Between Anlytical and Explicit and Implicit Methods of Solving One-

Dimensional Transient Heat Conduction Problems. *WSEAS Transactions on Heat and Mass Transfer*, Vol.1, No.4, (April 2006), pp. 567-571, ISSN 1790-5044

Shuja, S.Z.; Yilbas, B.S. & Khan, S.M. (2008). Laser Heating of Semi-Infinite Solid with Consecutive Pulses: Influence of Material Properties on Temperature Field. *Optics and Laser Technology*, Vol.40, No.3, (April 2008), pp. 472-480, ISSN 0030-3992

Steen, W.M. & Mazumder, J. (2010). *Laser Material Processing*, Springer-Verlag, ISBN 978-1-84996-061-8, London, Great Britain

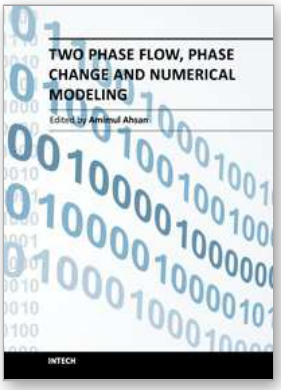


**Two Phase Flow, Phase Change and Numerical Modeling**

Edited by Dr. Amimul Ahsan

ISBN 978-953-307-584-6
Hard cover, 584 pages
**Publisher** InTech
**Published online** 26, September, 2011
**Published in print edition** September, 2011

The heat transfer and analysis on laser beam, evaporator coils, shell-and-tube condenser, two phase flow, nanofluids, complex fluids, and on phase change are significant issues in a design of wide range of industrial processes and devices. This book includes 25 advanced and revised contributions, and it covers mainly (1) numerical modeling of heat transfer, (2) two phase flow, (3) nanofluids, and (4) phase change. The first section introduces numerical modeling of heat transfer on particles in binary gas-solid fluidization bed, solidification phenomena, thermal approaches to laser damage, and temperature and velocity distribution. The second section covers density wave instability phenomena, gas and spray-water quenching, spray cooling, wettability effect, liquid film thickness, and thermosyphon loop. The third section includes nanofluids for heat transfer, nanofluids in minichannels, potential and engineering strategies on nanofluids, and heat transfer at nanoscale. The forth section presents time-dependent melting and deformation processes of phase change material (PCM), thermal energy storage tanks using PCM, phase change in deep CO2 injector, and thermal storage device of solar hot water system. The advanced idea and information described here will be fruitful for the readers to find a sustainable solution in an industrialized society.

**How to reference**

In order to correctly reference this scholarly work, feel free to copy and paste the following:

Marian Pearsica, Stefan Nedelcu, Cristian-George Constantinescu, Constantin Strimbu, Marius Benta and Catalin Mihai (2011). Modeling the Physical Phenomena Involved by Laser Beam – Substance Interaction, Two Phase Flow, Phase Change and Numerical Modeling, Dr. Amimul Ahsan (Ed.), ISBN: 978-953-307-584-6, InTech, Available from: http://www.intechopen.com/books/two-phase-flow-phase-change-and-numerical-modeling/modeling-the-physical-phenomena-involved-by-laser-beam-substance-interaction

INTECH
open science | open minds

**InTech Europe**
University Campus STeP Ri
Slavka Krautzeka 83/A
51000 Rijeka, Croatia
Phone: +385 (51) 770 447
Fax: +385 (51) 686 166
www.intechopen.com

**InTech China**
Unit 405, Office Block, Hotel Equatorial Shanghai
No.65, Yan An Road (West), Shanghai, 200040, China
中国上海市延安西路65号上海国际贵都大饭店办公楼405单元
Phone: +86-21-62489820
Fax: +86-21-62489821